Advances in Differential Equations and Control Processes 2025, 32(4), 3589.
doi: https://doi.org/10.59400/adecp3589

Article

Exact solutions of the (2+1)-dimensional BLMP equation via neural network-based symbolic computation

Jiang-Long Shen[1], Run-Fa Zhang[2,*], Jing-Wen Huang[1], Yu Gao[1], Jing-Bin Liang[1]

[1] School of Mathematics and Physics, Yibin University, Yibin 644000, China

[2] School of Automation and Software Engineering, Shanxi University, Taiyuan 030013, China

*** Corresponding author:** Run-Fa Zhang, zrf@sxu.edu.cn

CITATION

Shen J-L, Zhang R-F, Huang J-W, et al. Exact solutions of the (2+1)-dimensional BLMP equation via neural network-based symbolic computation. Advances in Differential Equations and Control Processes. 2025; 32(4): 3589. https://doi.org/10.59400/adecp3589

ARTICLE INFO

Received: 31 July 2025
Revised: 20 August 2025
Accepted: 20 September 2025
Available online: 1 December 2025

Abstract: This paper introduces a neural network-based symbolic computation framework for deriving exact analytical solutions to nonlinear partial differential equations (NLPDEs). By integrating the expressive capability of neural networks with the interpretability of symbolic methods, the approach offers a flexible, generalizable, and computationally efficient alternative to traditional techniques. Its architecture is straightforward, requiring minimal prior assumptions about the equation structure, thus enabling broad applicability across mathematical physics. As a case study, we investigate the (2+1)-dimensional Boiti-Leon-Manna-Pempinelli (BLMP) equation, a fundamental model describing wave propagation in fluid dynamics, nonlinear optics, and plasma physics. By systematically varying hidden-layer configurations and activation functions, we construct six distinct neural network models—comprising both single- and double-hidden-layer designs. These yield multiple novel exact analytical solutions, revealing diverse dynamic behaviors such as localized wave structures, periodic oscillations, and energy-localized modes. The physical characteristics of the obtained solutions are visualized through three-dimensional surface plots, contour maps, density distributions, and temporal evolution graphs. These illustrations elucidate key features including waveform stability, soliton localization, and nonlinear interactions. Unlike conventional methods such as the Hirota bilinear transformation or inverse scattering, the proposed framework avoids complex algebraic manipulations and does not rely on specialized transformations. Compared to physics-informed neural networks, it achieves higher interpretability and reduced computational dependency. This work expands the solution space of the (2+1)-dimensional BLMP equation and highlights the potential of neural-symbolic computation for discovering exact solutions in complex nonlinear systems.

Keywords: (2+1)-dimensional BLMP equation; neural networks; nonlinear partial differential equations; symbolic computation; lump solution

1. Introduction

Nonlinear partial differential equations are widely used in physics, oceanography and various engineering fields [1–6]. By solving the exact solution of nonlinear partial differential equations, we can have a deeper understanding and explore the properties hidden behind the equations, thus guiding engineering practice to better serve social development. The emergence of nonlinear partial differential equations and complex boundary conditions has driven the development of novel solution methods.

Meanwhile, advancements in computational technology have facilitated the verification of exact solutions.

At present, there are multiple effective approaches for solving exact solutions of nonlinear partial differential equations. In nonlinear mathematical physics, common classical methods include the homogeneous balance method [7], inverse scattering transformation [8], Bäcklund transformation [9], Hirota bilinear transformation [10–12], Lie group analysis [13, 14], and Darboux transformation [15]. The Broer-Ling-Ma-Proudman (BLMP) equation is a fundamental nonlinear partial differential equation that has been widely studied in physics and engineering, especially for its role in modeling wave propagation in fluid dynamics and nonlinear systems. In fluid mechanics, the equation can be used to simulate and study complex nonlinear wave phenomena in incompressible fluids, which helps to gain a deeper understanding of the complex phenomena and laws in fluid dynamics [16]; in the field of optical fiber communications, the BLMP equation can be employed to characterize the nonlinear transmission properties of light pulses in optical fibers, providing theoretical support for long-distance transmission and stable control of optical signals; in plasma physics [17], the BLMP equation can describe certain specific nonlinear wave modes in plasma.

This paper will study the (2+1)-dimensional BLMP equation, which was first proposed by Gilson et al. [18, 19] in 1993 to describe the one-dimensional interaction and long-wave propagation of (2+1)-dimensional Riemann waves along the x-axis and y-axis.

$$u_t + u_{xxx} + u_{yyy} = 0 \tag{1}$$

In recent years, research on the BLMP equation has flourished, and researchers have made a series of encouraging progress [20–24]. These studies have explored various analytical and numerical techniques, such as bilinear methods, symmetry reductions, and methods based on physical information, to derive exact solutions. Qin et al. [25] used the Hirota bilinear method to solve the multi-soliton solutions of the (2+1)-dimensional BLMP equation. Shen et al. [26] studied the multi-soliton solutions of the (3+1)-dimensional BLMP equation using a bilinear neural network method. Zhang et al. [27] successfully solved the soliton solution and periodic solution of the BLMP equation using the Hirota bilinear method and the Riemann theta function method, and deepened their understanding of the mathematical properties of the BLMP equation through Painlevé analysis and Bäcklund transformation. Kumar et al. [2] used the generalized exponential rational function method to construct multiple closed-form solutions by converting the BLMP equation into an ordinary differential equation. Bilige et al. [28] obtained multiple closed-form solutions to the fractional (3+1)-dimensional BLMP equation by using the generalized exponential rational function method (GERF) and the Hirota bilinear method.

In addition, Raissi et al. introduced a physical information neural network in 2019 [29]. This approach harnesses deep learning to integrate physical data seamlessly into the model. It bypasses conventional numerical discretization techniques.

Additionally, it offers a versatile framework for tackling partial differential equations. This is particularly effective when addressing intricate physical challenges. Wang et al. [30] developed innovative methods, including adaptive weight tuning. They also enhanced sampling techniques and optimized network structures. These improvements boost training efficiency and solution precision in Physics-Informed Neural Networks (PINNs). Furthermore, they confirmed the method's effectiveness across various partial differential equation problems. Mishra et al. [31] conducted an in-depth theoretical analysis of the generalization error of physical information neural networks (PINNs) in solving the inverse problem of a class of partial differential equations, derived the bounds of approximation, optimization and statistical errors, and revealed the key factors affecting the error.

Whether based on traditional methods or physical information, neural network models developed based on tools such as machine learning, extensive attempts have been made and fruitful results have been achieved in the field of studying exact solutions of partial differential equations [32, 33]. However, there are still problems that cannot be ignored. For example, machine learning or physical information neural network methods usually need to seek a balance between solution accuracy and computing resource requirements. Although physical information neural networks have made great progress, they still face challenges in computational efficiency, computational accuracy, and model complexity. However, they usually require complex processes or a large amount of computing resources, which limits their practicality. Although traditional mathematical methods have high solution accuracy, they are highly dependent on the mathematical background of researchers. In this study, we introduce an innovative approach that harnesses direct neural network symbolic processing (**Figure 1**). We have devised two primary neural network architectures: the Model[3-3-1] (**Figure 2a**) and the Model[3-3-2-1] (**Figure 2b**), and combined them with diverse activation functions to generate six unique configurations. By constructing different trial functions, we have successfully obtained multiple exact analytical solutions for the (2+1)-dimensional BLMP equation. This method stands out for its simplicity and effectiveness compared to existing approaches. Compared to the bilinear neural network method, our approach eliminates the need for complex bilinear transformations, significantly reducing the difficulty and entry barriers for researchers. This makes it highly adaptable for applications in physics, engineering, and beyond. In contrast to the physical information neural network (PINN) method, our technique achieves superior accuracy with lower dependency on computational hardware, enhancing its practicality. We have already derived solutions for different models and generated corresponding visualizations, which will be elaborated in subsequent sections.

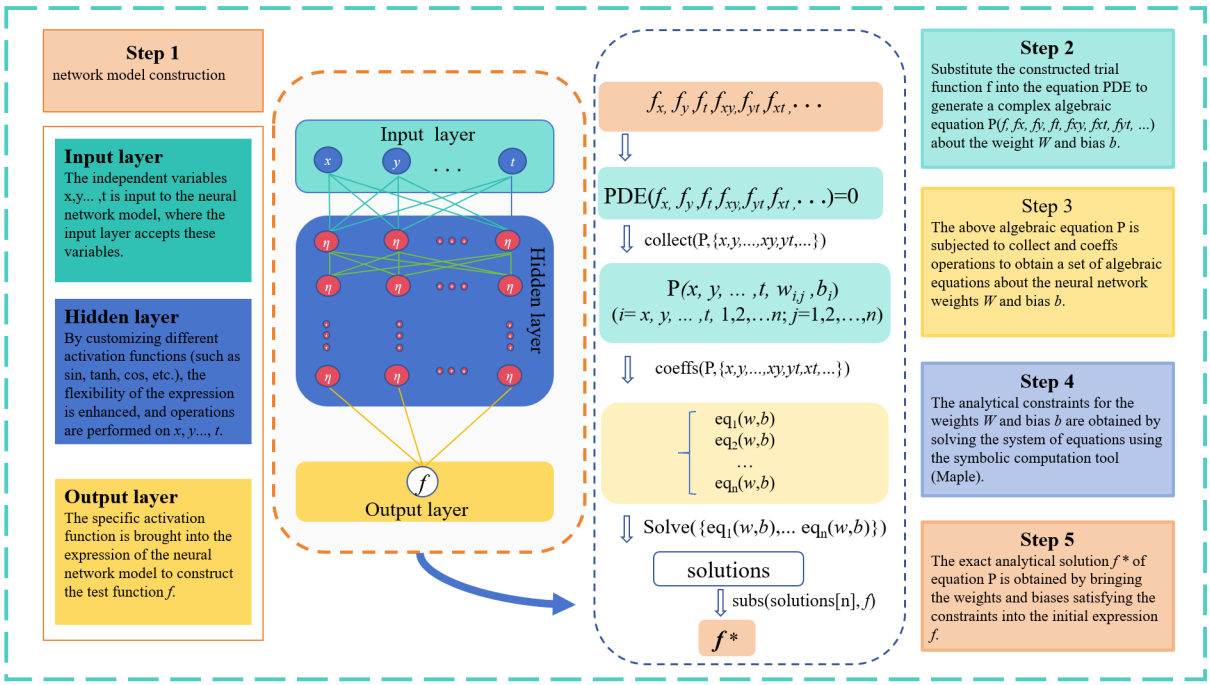

Figure 1. Neural network symbolic computation flow chart.

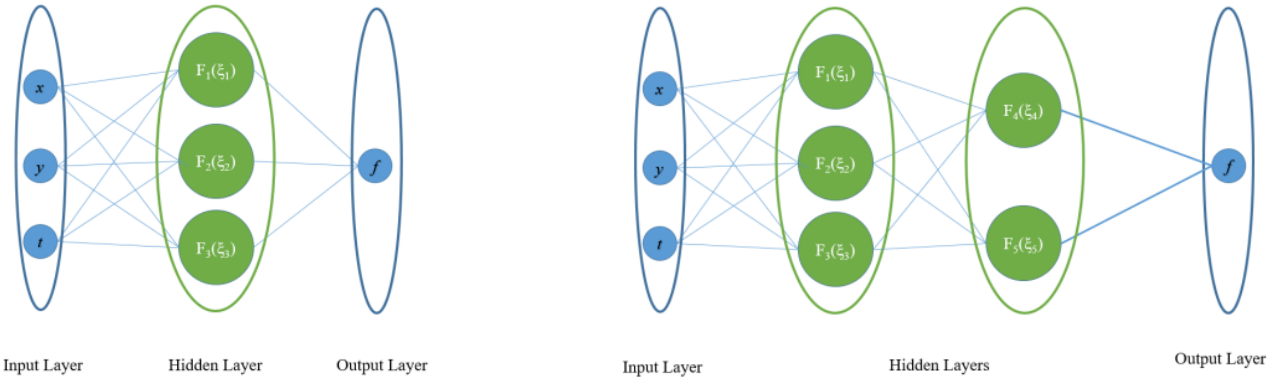

(a) Single Hidden Layer Network. **(b)** Double Hidden Layer Network.

Figure 2. The neural network model.

2. Symbolic computation model based on a neural network

The symbolic computation approach grounded in neural networks represents an advancement over the bilinear neural network technique proposed by Xie et al. [34]. This method, termed BNNM, has effectively addressed a diverse array of partial differential equations. In contrast to BNNM and conventional methodologies, this technique exhibits robust generalization and broad applicability. The procedure encompasses five distinct phases (**Figure 1**): Initially, a neural network model is formulated, employing its derived expression to encapsulate the underlying function of the nonlinear partial differential equation. Subsequently, this expression is integrated into the target nonlinear partial differential equation, yielding a sophisticated algebraic formulation. The next step involves extracting the coefficients associated with the independent variable and its derivatives from this algebraic form, thus establishing a set of algebraic equations. These equations are then resolved to determine constraints

exclusively on the weight 'W' and the threshold 'b'. Finally, these constraints are incorporated into the initial expression to derive the precise solution to the nonlinear partial differential equation.

$$\begin{gathered} f = W_{1,f}F_1(\xi_1) + W_{2,f}F_2(\xi_2) + W_{3,f}F_3(\xi_3) + b_4 \\ \xi_i = W_{x,i}x + W_{y,i}y + W_{t,i}t + b_i, (i = 1,\ 2,\ 3) \end{gathered} \tag{2}$$

$$\begin{gathered} f = \sum_4^5 W_{n,f}F_n(\xi_n) + b_6, \\ \xi_i = W_{1,i}F_1(\xi_1) + W_{2,i}F_2(\xi_2) + W_{3,i}F_3(\xi_3),\ (i = 4, 5), \\ \xi_1 = W_{x,1}x + W_{t,1}t + b_5, \\ \xi_2 = W_{x,2}x + W_{t,2}t + b_4, \\ \xi_3 = W_{x,3}x + W_{t,3}t + b_3 \end{gathered} \tag{3}$$

Equations (2) and (3) are expressions constructed by the single hidden layer neural network model (**Figure 2a**) and the double hidden layer neural network model (**Figure 2b**), respectively. Based on these two core neural network architectures, Model[3-3-1] and Model[3-3-2-1], six different network configurations were constructed by adopting different activation function combination strategies. Six different trial function expressions were obtained.

3. Single hidden layer model

3.1. Model[3-3-1]-1

In order to solve the (2+1)-dimensional BLMP equation Equation (1), we choose a single hidden layer neural network model (**Figure 1a**): 3 neurons in the input layer and 3 neurons in the hidden layer $F_1(\xi_1)$, $F_2(\xi_2)$, $F_3(\xi_3)$. Letting $F_1(\xi_1) = sech(\xi_1)^2$, $F_2(\xi_2) = \sin(\xi_2)$,$F_3(\xi_3) = \cos(\xi_3)$ in **Figure 1a**, and according to the analytical formulation provided by the deep neural network Model[3-3-3]-1, we are able to derive:

$$\begin{aligned} f \ &= b_4 + w_{1,u}\, sech(t \cdot w_{t,1} + x \cdot w_{x,1} + y \cdot w_{y,1} + b_2)^2 \\ &+ w_{2,u} \sin(t \cdot w_{t,2} + x \cdot w_{x,2} + y \cdot w_{y,2} + b_3) \\ &+ w_{3,u} \cos(t \cdot w_{t,3} + x \cdot w_{x,3} + y \cdot w_{y,3} + b_5) \end{aligned} \tag{4}$$

Insert Equation (4) into the nonlinear PDE (1), and a solution can be derived.

$$\begin{gathered} \{w_{1,u} = 0, w_{2,u} = w_{2,u}, w_{3,u} = w_{3,u}, w_{t,1} = w_{t,1}, w_{x,1} = w_{x,1}, \\ w_{y,1} = w_{y,1}, w_{t,2} = w_{x,2}^3 + w_{x,2}w_{y,2}^2, w_{x,2} = w_{x,2}, w_{y,2} = w_{y,2}, \\ w_{t,3} = w_{x,3}^3 + w_{x,3}w_{y,3}^2, w_{x,3} = w_{x,3}, w_{y,3} = w_{y,3}\} \end{gathered} \tag{5}$$

By inserting Equation (5) into Equation (4), the resolution of the initial equation can be derived as:

$$\begin{aligned} f \ &= b_4 + w_{2,u} \sin\left(tw_{x,2}^3 + (tw_{y,2}^2 + x)w_{x,2} + yw_{y,2} + b_3\right) \\ &+ w_{3,u} \cos\left(tw_{x,3}^3 + (tw_{y,3}^2 + x)w_{x,3} + yw_{y,3} + b_5\right) \end{aligned} \tag{6}$$

In order to show the dynamic characteristics of the solution, we assign values to the parameters and use Maple to generate images. **Figure 3** shows the image of

the solution after the parameters are assigned. It includes three-dimensional graphs, contour diagrams, thermal maps, and evolution plots, which fully show the dynamic characteristics of the solution. Based on the multi-angle visualizations in **Figure 3**, the dynamic characteristics of the physical field governed by Equation (6) are clearly illustrated. This analytical solution represents a nonlinear periodic wave train propagating in (2+1)-dimensional spacetime. The plots collectively confirm its fundamental physical properties, including waveform preservation, energy localization, and stable periodic oscillation during propagation.

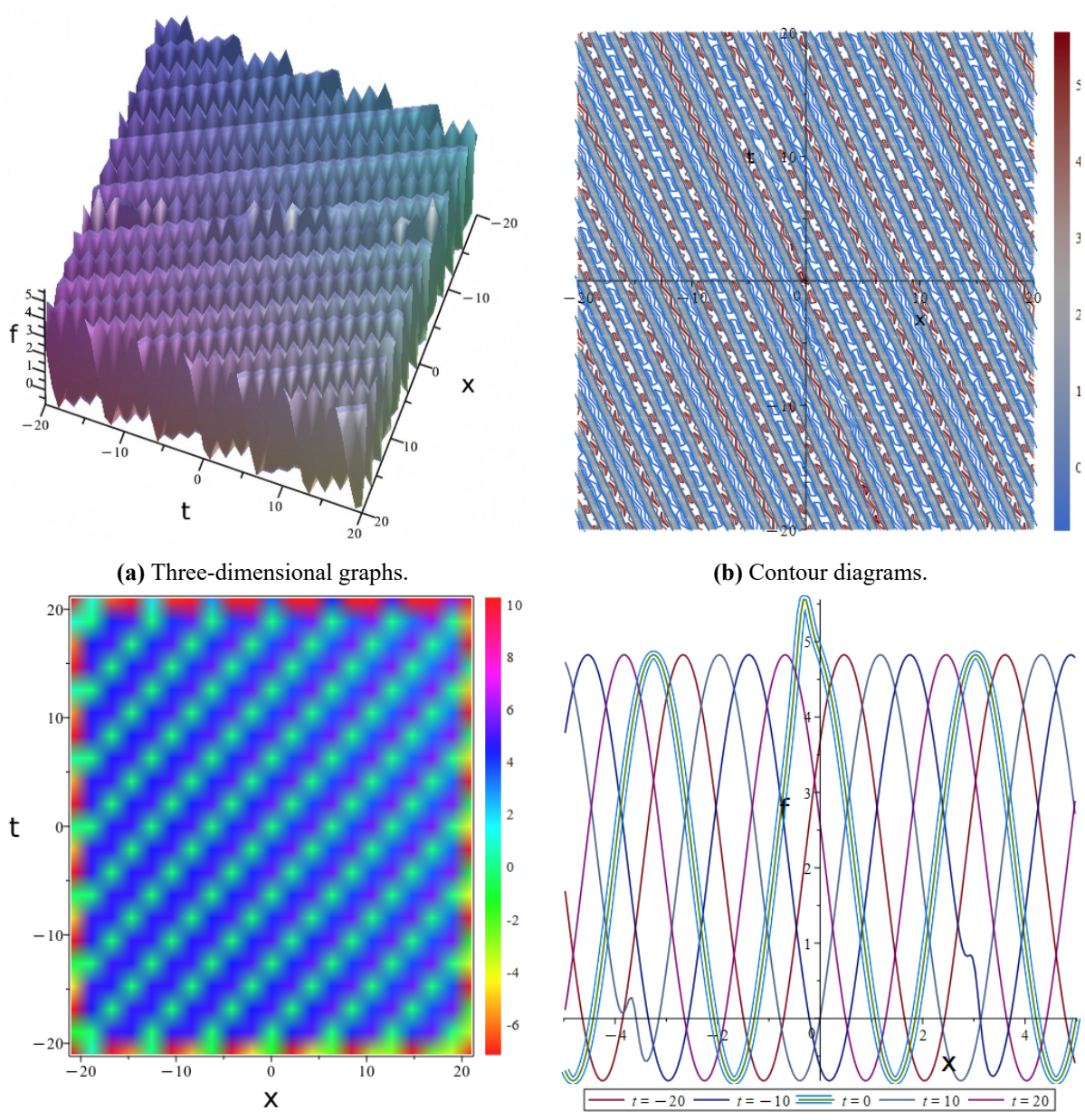

(a) Three-dimensional graphs.

(b) Contour diagrams.

(c) Thermal maps.

(d) Evolution plot.

Figure 3. Three-dimensional graphs, contour diagrams, thermal maps, and evolution plot of Equation (6) at: $b_3 = 1, b_5 = 1, b_4 = 2, w_{t,1} = 2, w_{x,1} = 1, w_{y,1} = 3, b_2 = 2, w_{2,u} = 2,\ w_{1,u} = 1, w_{3,u} = 2, w_{t,2} = 1, w_{t,3} = 1, w_{x,2} = 1, w_{x,3} = 1$.

3.2. Model[3-3-1]-2

To derive various analytical solutions using the single hidden layer network, we modified the activation function within the hidden layer. Assigning $F_1(\xi_1) = \text{sech}(\xi_1)^2$, $F_2(\xi_2) = \sin(\xi_2)$, and $F_3(\xi_3) = \tanh(\xi_3)$ as shown in **Figure 2a**, and following the analytical framework offered by the deep neural network Model[3-3-3]-2, we can derive:

$$\begin{aligned} f \quad &= b_4 + w_{1,u}\,\text{sech}\,(t\cdot w_{t,1} + x\cdot w_{x,1} + y\cdot w_{y,1} + b_2)^2 \\ &+ w_{2,u}\,\sin(t\cdot w_{t,2} + x\cdot w_{x,2} + y\cdot w_{y,2} + b_3) \\ &+ w_{3,u}\,\tanh(t\cdot w_{t,3} + x\cdot w_{x,3} + y\cdot w_{y,3} + b_5) \end{aligned} \tag{7}$$

Insert Equation (7) into the nonlinear PDE(1), and a solution can be derived.

$$\begin{gathered} \{w_{1,u} = w_{1,u}, w_{2,u} = w_{2,u}, w_{3,u} = 0,\ w_{t,1} = 0, w_{t,2} = w_{x,2}^3 + w_{x,2}w_{y,2}, \\ w_{t,3} = w_{t,3}, w_{x,1} = 0, w_{x,2} = w_{x,2}, w_{x,3} = w_{x,3}, w_{y,1} = w_{y,1}, \\ w_{t,3} = w_{t,3}, w_{x,1} = 0, w_{x,2} = w_{x,2}, w_{x,3} = w_{x,3}, w_{y,1} = w_{y,1}, \\ w_{y,2} = w_{y,2}, w_{y,3} = w_{y,3}\} \end{gathered} \tag{8}$$

By substituting Equation (8) into Equation (7) the solution of the original equation can be obtained as:

$$\begin{aligned} f \quad &= b_4 + w_{1,u}\,sech\,(yw_{y,1} + b_2)^2 \\ &+ w_{2,u}\sin\left(tu_{x,2}^3 + (tw_{y,2}^2 + x)w_{x,2} + yw_{y,2} + b_3\right) \end{aligned} \tag{9}$$

Figure 4 illustrates the dynamic characteristics of the soliton-supported periodic wave from multiple perspectives: **Figure 4a** displays the overall spatial structure of the composite wave in three dimensions, revealing a complex waveform that combines background distortion induced by the soliton component and regular oscillations arising from the periodic component. **Figure 4b,c** depict the energy distribution of the wave through a contour diagram and a thermal map, respectively. Both visualizations clearly exhibit a complex interference pattern resulting from the superposition of the soliton and periodic wave components. **Figure 4d** presents the temporal evolution of the waveform, highlighting the coexistence of an overall envelope propagating at the soliton velocity and rapidly oscillating periodic waves within it. The existence of this analytical solution demonstrates that highly localized soliton modes and spatially extended periodic wave modes can stably coexist in the system. The soliton component facilitates energy localization, while the periodic wave component likely mediates energy transfer and exchange. Moreover, the structural stability of the solution during propagation suggests that this wave interaction represents an intrinsic eigenmode of the system. These findings are essential for understanding long-term wave behaviors in real-world physical systems described by the BLMP equation.

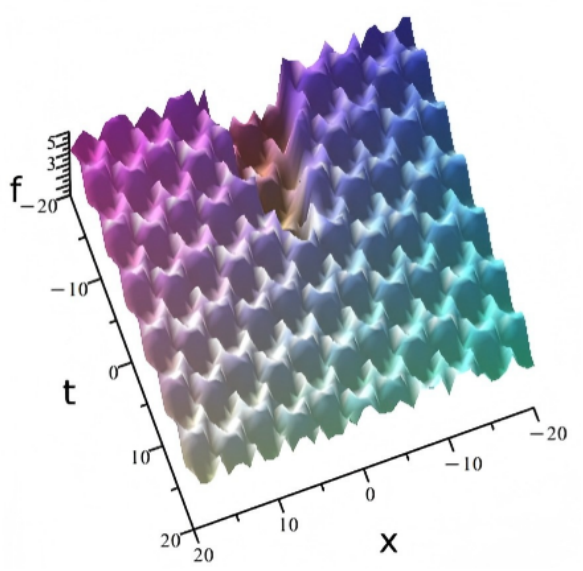

(a) Three-dimensional graphs.

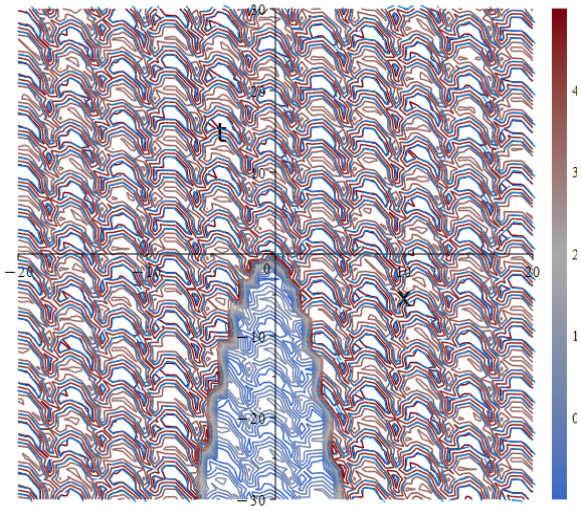

(b) Contour diagrams.

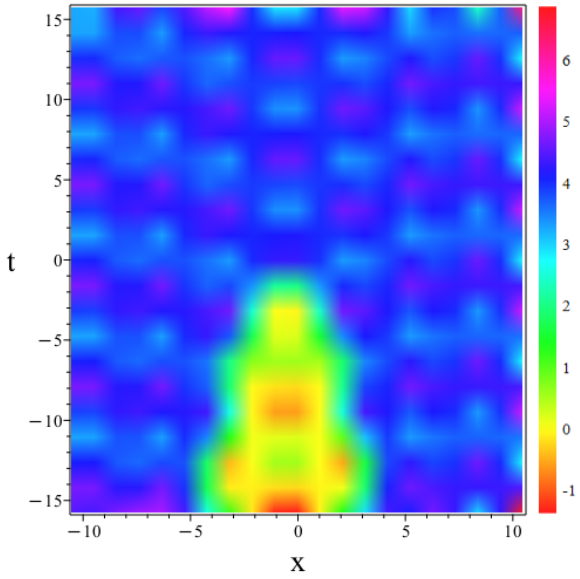

(c) Thermal maps.

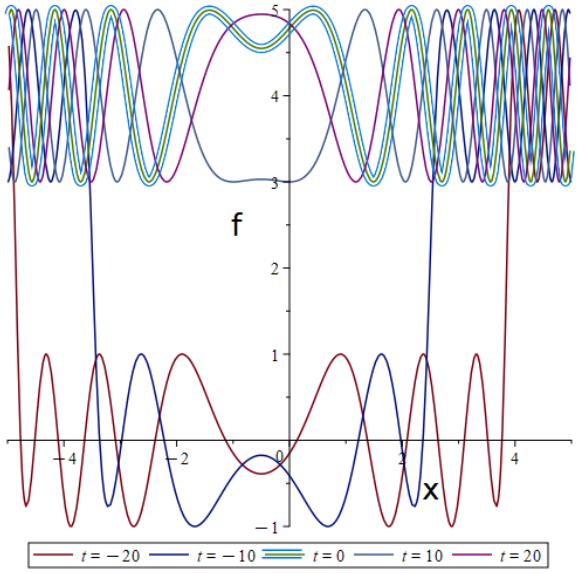

(d) Evolution plot.

Figure 4. Three-dimensional graphs, contour diagrams, thermal maps, and evolution plot of Equation (9) at : $b_3 = 1, b_2 = 1, b_5 = 1, b_4 = 2, w_{t,1} = 1, w_{x,1} = 1, w_{y,1} = 1, w_{2,u} = 1,\ w_{1,u} = 1, w_{y,2} = 1, w_{3,u} = 2, w_{t,2} = 1, w_{t,3} = 1, w_{x,2} = 1, w_{x,3} = 1,\ w_{y,3} = 1.$

3.3. Model[3-3-1]-3

To derive a variety of analytical solutions utilizing the single hidden layer network, we optimized the activation function within the concealed layer. Assigning $F_1(\xi_1) = \text{sech}(\xi_1)^2$, $F_2(\xi_2) = \sin(\xi_2)$, and $F_3(\xi_3) = \cosh(\xi_3)$ as depicted in **Figure 2a**, and in accordance with the theoretical framework supplied by the deep neural network Model[3-3-3]-3, we can derive:

$$\begin{aligned} f \quad &= b_4 + w_{1,u}\,\text{sech}\,(t\cdot w_{t,1} + x\cdot w_{x,1} + y\cdot w_{y,1} + b_2)^2 \\ &+ w_{2,u}\sin(t\cdot w_{t,2} + x\cdot w_{x,2} + y\cdot w_{y,2} + b_3) \\ &+ w_{3,u}\cosh(t\cdot w_{t,3} + x\cdot w_{x,3} + y\cdot w_{y,3} + b_5) \end{aligned} \tag{10}$$

Insert Equation (10) into the nonlinear PDE(1), and a solution can be derived.

$$\begin{gathered}\{w_{1,u}=0, w_{3,u}=w_{3,u}\ , w_{t,1}=w_{t,1}, w_{t,2}=w_{t,2}, w_{t,3}= \\ -w_{x,3}^3-w_{x,3}w_{y,3}^2, w_{2,u}=0, w_{x,1}=w_{x,1}, w_{x,2}= \\ w_{x,2}, w_{x,3}=w_{x,3}, w_{y,1}=w_{y,1}, w_{y,2}=w_{y,2}, w_{y,3}=w_{y,3}\}\end{gathered} \tag{11}$$

By inserting Equation (11) into Equation (10), the resolution of the initial equation can be derived as:

$$f=b_4+w_{3,u}\cosh\left(-tw_{x,3}^3+(-tw_{y,3}^2+x)w_{x,3}+yw_{y,3}+b_5\right) \tag{12}$$

Based on the analytical solution (12) and its visualization results (see **Figure 5**), the solution describes a transient high-energy pulse propagating in space. Its waveform exhibits obvious energy concentration characteristics during propagation, manifested as a moving localized peak. This peak first strengthens and then weakens over time, demonstrating the dynamic process of energy accumulation and dissipation in a nonlinear system.

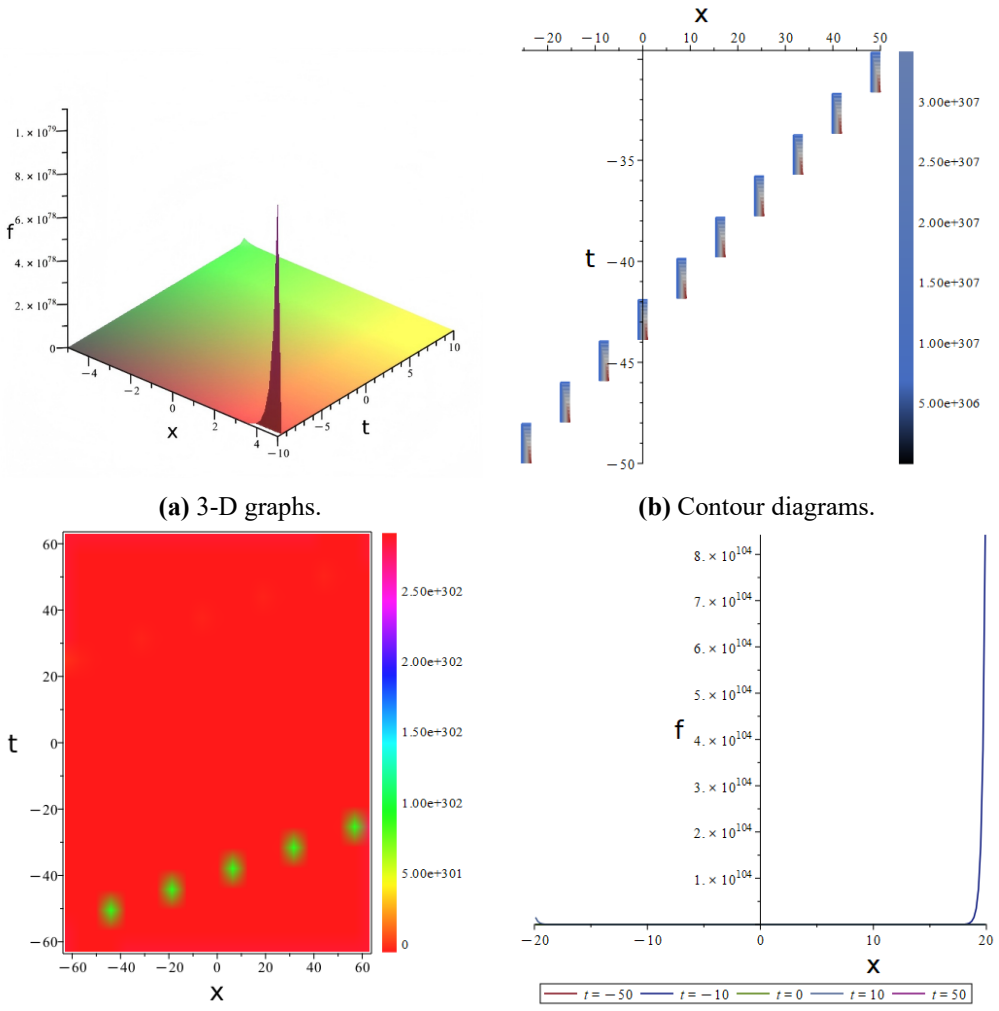

(a) 3-D graphs. **(b)** Contour diagrams.

(c) Thermal maps. **(d)** Evolution plot.

Figure 5. Three-dimensional graphs, contour diagrams, thermal maps, and evolution plot of Equation (12) at: $b_4=2,\ w_{3,u}=2,\ w_{x,3}=2, w_{y,3}=2, b_5=2.$

4. Double hidden layer model

4.1. Model[3-3-2-1]-1

Unlike the single hidden layer network in the previous section, in this section, we increase the number of hidden layers to two. By increasing the number of hidden layers, we can enhance the expression and generalization capabilities of the neural network model and improve the optimization effect of the model. In order to solve the (2+1)-dimensional BLMP equation Equation (1), we choose a double hidden layer neural network model (**Figure 2b**): 3 neurons in the input layer, 3 neurons in the first hidden layer, and 2 neurons in the second hidden layer, the output layer has 1 neuron. $F_1(\xi_1)$, $F_2(\xi_2)$, $F_3(\xi_3)$, $F_4(\xi_4)$, $F_5(\xi_5)$. Letting $F_1(\xi_1) = \xi_1$, $F_2(\xi_2) = \xi_2$, $F_3(\xi_3) = (\xi_3)$, $F_4(\xi_4) = \tanh(\xi_4)$, $F_5(\xi_5) = \cos(\xi_5)$ in **Figure 2b**, and according to the analytical formulation provided by the deep neural network Model[3-3-2-1]-1, we are able to derive.

$$\begin{aligned} f \quad &= b_6 + w_{4,u} \cdot \tanh(w_{t,4}(t \cdot w_{t,1} + xw_{x,1} + yw_{y,1}) \\ &+ w_{2,4} \cdot (t \cdot w_{t,2} + x \cdot w_{x,2} + yw_{y,2}) \\ &+ w_{3,4} \cdot (t \cdot w_{t,3} + x \cdot w_{x,3} + yw_{y,3}) \\ &+ w_{5,u} \cdot \cos(w_{1,5} \cdot (t \cdot w_{t,1} + xw_{x,1} + yw_{y,1}) \\ &+ w_{2,5} \cdot (t \cdot w_{t,2} + x \cdot w_{x,2} + yw_{y,2}) \\ &+ w_{3,5} \cdot (t \cdot w_{t,3} + x \cdot w_{x,3} + yw_{y,3}) \end{aligned} \tag{13}$$

$$\begin{aligned} &\{w_{1,4} = 0, w_{1,5} = 0, w_{2,4} = w_{2,4}, w_{2,5} = w_{2,5}, w_{3,4} = w_{3,4}, w_{3,5} = w_{3,5}, \\ &w_{t,1} = \tfrac{1}{w_{2,4}^3 w_{1,5}} \left(w_{1,5}^3 w_{2,4}^3 w_{x,1}^3 + w_{1,5}^3 w_{2,4}^3 w_{x,1} w_{y,1}^2\right) \\ &+2w_{1,5}^2 w_{2,4}^3 w_{2,5} w_{x,1} w_{y,1} w_{y,2} + 3w_{1,5}^2 w_{2,4}^3 w_{3,5} w_{x,1}^2 w_{x,3} \\ &+2w_{1,5}^2 w_{2,4}^3 w_{3,5} w_{x,1} w_{y,1} w_{y,3} + w_{1,5}^2 w_{2,4}^3 w_{3,5} w_{x,3} w_{y,1}^2 \\ &-3w_{1,5}^2 w_{2,4}^2 w_{2,5} w_{3,4} w_{x,1} w_{x,3} - w_{1,5}^2 w_{2,4}^2 w_{2,5} w_{3,4} w_{x,3} w_{y,1} \\ &+w_{1,5} w_{2,4}^3 w_{2,5}^2 w_{x,1} w_{y,2}^2 + 2w_{1,5} w_{2,4}^3 w_{2,5} w_{3,5} w_{x,1} w_{y,2} w_{y,3} \\ &+2w_{1,5} w_{2,4}^3 w_{2,5} w_{3,5} w_{x,3} w_{y,1} w_{y,3} + 3w_{1,5} w_{2,4}^3 w_{3,5} w_{x,1} w_{x,3}^2 \\ &+w_{1,5} w_{2,4}^3 w_{3,5} w_{x,1} w_{y,3}^2 + 2w_{1,5} w_{2,4}^3 w_{3,5} w_{x,3} w_{y,1} w_{y,3} \\ &-2w_{1,5} w_{2,4}^2 w_{2,5}^2 w_{3,4} w_{x,1} w_{x,3} - 6w_{1,5} w_{2,4}^2 w_{2,5} w_{3,4} w_{3,5} w_{x,1} w_{x,3} \\ &-2w_{1,5} w_{2,4}^2 w_{2,5} w_{3,4} w_{3,5} w_{x,3} w_{y,1} + 3w_{1,5} w_{2,4} w_{2,5}^2 w_{3,4} w_{x,1} w_{x,3} \\ &+2w_{2,4}^3 w_{2,5}^2 w_{3,5} w_{x,3} w_{y,2} w_{y,3} + w_{2,4}^3 w_{3,5}^3 w_{x,3}^3 + w_{2,4}^3 w_{3,5}^3 w_{x,3} w_{y,3}^2 \\ &-w_{2,4}^2 w_{2,5}^3 w_{3,4}^3 w_{x,3}^3 - 2w_{2,4}^2 w_{2,5}^3 w_{3,4}^3 w_{x,3} w_{y,3}^2 - 2w_{2,4}^2 w_{2,5}^2 w_{3,4}^3 w_{3,5}^3 w_{x,3}^3 \\ &-w_{2,4}^2 w_{2,5}^2 w_{3,4}^3 w_{3,5}^3 w_{x,3} w_{y,3}^2 - 3w_{2,4}^2 w_{2,5}^3 w_{3,4}^2 w_{3,5}^3 w_{x,3}^3 \\ &-3w_{2,4}^3 w_{2,5}^3 w_{3,4}^3 w_{x,3}^3 \\ &w_{t,2} = -\tfrac{w_{3,4}^4 w_{t,3}^3}{w_{2,4}^3}, w_{t,3} = w_{t,3}, w_{x,1} = w_{x,1}, w_{x,2} = -\tfrac{w_{3,4}^3 w_{x,3}^3}{w_{2,4}^2} \\ &w_{x,3} = w_{x,3}, w_{y,1} = w_{y,1}, w_{y,2} = w_{y,2}, w_{y,3} = w_{y,3} \\ &w_{4,u} = w_{4,u}, w_{5,u} = w_{5,u}\} \end{aligned} \tag{14}$$

By substituting Equation (14) into Equation (13), we are able to derive the

resolution of the initial equation as:

$$\begin{aligned} f \quad &= b_6 + w_{4,u}\tanh\left(y(w_{2,4}w_{y,2} + w_{3,4}w_{y,3})\right) \\ &+ w_{5,u}\cos(\tfrac{1}{w_{2,4}^3}((w_{x,3}^2 w_{3,5}^2 + 2w_{1,5}w_{3,5}w_{x,1}w_{x,3} + w_{y,3}^2 w_{3,5}^2 \\ &+ 2w_{y,3}(w_{1.5}w_{y,1} + w_{2.5}w_{y,2})w_{3.5} + (w_{x,1}^2 + w_{y,1}^2)w_{1.5}^2 \\ &+ 2w_{y,1}w_{y,2}w_{1.5}w_{2.5} + w_{y,2}^2 w_{2.5}^2)(w_{1.5}w_{x,1} + w_{3.5}w_{x,3})t \\ &+ xw_{3,5}w_{x,3} + yw_{3,5}w_{y,3} + (xw_{x,1} + yw_{y,1})w_{1,5} + w_{2,5}yw_{y,2})w_{2,4}^3 \\ &- 3w_{x,3}w_{3,4}((w_{x,3}^2 w_{3,5}^2 + 2w_{1,5}w_{3,5}w_{x,1}w_{x,3} + \tfrac{w_{y,3}^2 w_{3,5}^2}{3} \\ &+ \tfrac{2w_{y,3}(w_{1.5}w_{y,1} + w_{2.5}w_{y,2})w_{3.5}}{3} + (\tfrac{w_{y,1}^2}{3} + w_{x,1}^2)w_{1.5}^2 \\ &+ \tfrac{2w_{y,1}w_{y,2}w_{1,5}w_{2,5}}{3} + \tfrac{w_{y,2}^2 w_{2,5}^2}{3})t + \tfrac{x}{3})w_{2,5}w_{2,4}^2 \\ &+ 3tw_{x,3}^2 w_{2,5}^2 w_{3,4}^2(w_{1,5}w_{x,1} + w_{3,5}w_{x,3})w_{2,4} - tw_{2,5}^3 w_{3,4}^3 w_{x,3}^3) \end{aligned} \tag{15}$$

Combining the four sub-plots of Equation (15) in **Figure 6** Comprehensive analysis shows that this solution describes a weakly turbulent state dominated by nonlinearity under specific parameters. Its essence is the spatiotemporal chaotic behavior generated by the strong nonlinear interaction of wave modes at different scales, reflecting the dynamic characteristics of the system's transition from order to turbulence.

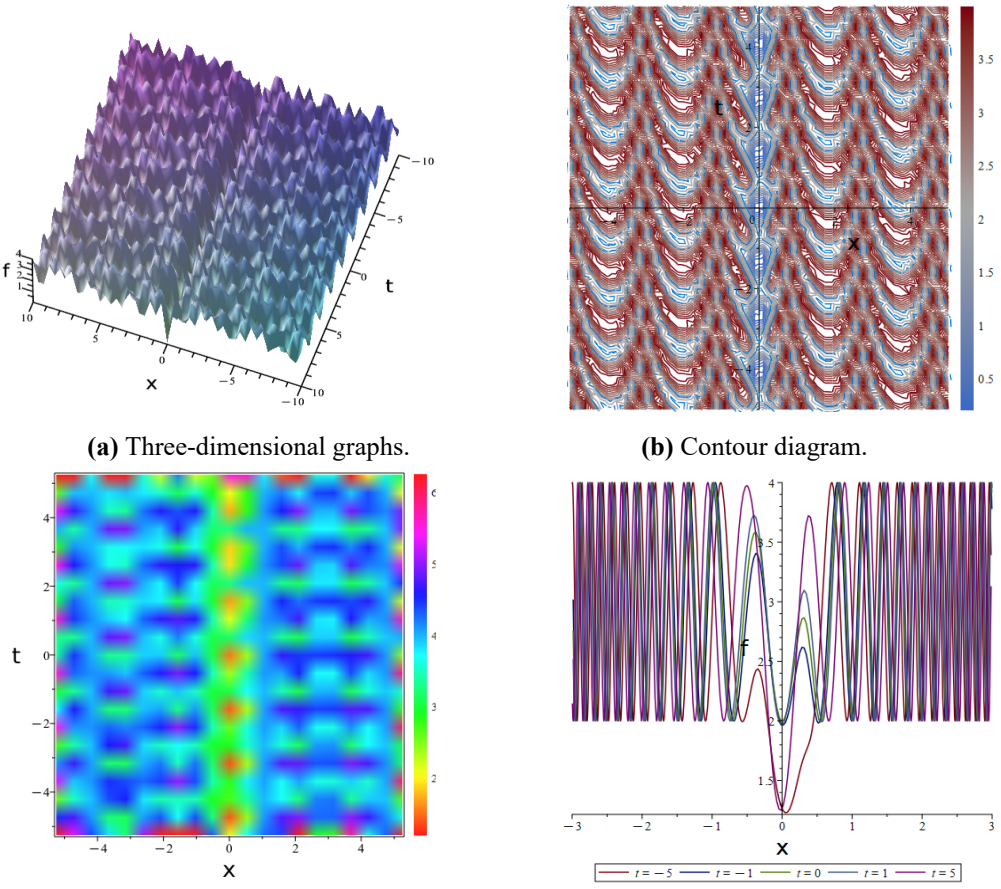

(a) Three-dimensional graphs. **(b)** Contour diagram.

(c) Thermal map. **(d)** Evolution plot.

Figure 6. Three-dimensional graphs, contour diagram, thermal map, and evolution plot of Equation (15) at $b_6 = 1, w_{4,u} = 2, w_{1,4} = 2, w_{y,1} = 2, w_{2,4} = 3, w_{y,2} = 2, w_{3,4} = 2, w_{y,3} = 2, w_{1,5} = 1, w_{3,5} = 1, w_{5,u} = 1, w_{2,5} = 2, w_{x,1} = 2, w_{x,3} = 2$.

4.2. Model[3-3-2-1]-2

In order to obtain different analytical solutions in the neural network model with the same number of layers, we combined and transformed the activation function of the second hidden layer. The activation function of the first hidden layer remains unchanged, and the activation function of the second hidden layer is adjusted. Letting $F_4(\xi_4) = \sin(\xi_4)$, $F_5(\xi_5) = \operatorname{sech}(\xi_5)$. By the deep neural network Model[3-3-2-1]-2, we can obtain:

$$\begin{aligned} f \quad &= b_6 + w_{4,u} \cdot \sin(w_{t,4}(t \cdot w_{t,1} + x w_{x,1} + y w_{y,1}) \\ &+ w_{2,4} \cdot (t \cdot w_{t,2} + x \cdot w_{x,2} + y w_{y,2}) \\ &+ w_{3,4} \cdot (t \cdot w_{t,3} + x \cdot w_{x,3} + y w_{y,3}) \\ &+ w_{5,u} \cdot sech\,(w_{1,5} \cdot (t \cdot w_{t,1} + x w_{x,1} + y w_{y,1}) \\ &+ w_{2,5} \cdot (t \cdot w_{t,2} + x \cdot w_{x,2} + y w_{y,2}) \\ &+ w_{3,5} \cdot (t \cdot w_{t,3} + x \cdot w_{x,3} + y w_{y,3}) \end{aligned} \tag{16}$$

Substitute Equation (16) into nonlinear PDE (1), 3 solutions can be obtained, one of the solutions is as follows,

$$\begin{gathered} \{w_{1,4} = 0, w_{1,5} = w_{1,5}, w_{2,4} = 0, w_{2,5} = w_{2,5}, w_{3,4} = w_{3,4}, w_{3,5} = w_{3,5} \\ w_{4,u} = w_{4,u}, w_{5,u} = w_{5,u} \\ w_{\ell,1} = -\frac{w_{3,4}^2 w_{3,5} w_{x,3}^3 + w_{3,4}^2 w_{3,5} w_{x,3} w_{y,3}^2 + w_{2,5} w_{t,2}}{w_{1,5}} \\ w_{\ell,2} = w_{\ell,2}, w_{\ell,3} = w_{3,4}^2 w_{x,3}^3 + w_{3,4}^2 w_{x,3} w_{y,3}^2 \\ w_{x,1} = -\frac{w_{2.5} w_{x,2} + w_{3.5} w_{x,3}}{w_{1.5}}, w_{x,2} = w_{x,2}, w_{x,3} = w_{x,3} \\ w_{y,1} = w_{y,1}, w_{y,2} = w_{y,2}, w_{y,3} = w_{y,3}\} \end{gathered} \tag{17}$$

By substituting Equation (17) into Equation (16), the solution of the original equation can ultimately be obtained as:

$$\begin{aligned} f: \quad &= b_6 + w_{4,u} \sin\left(w_{3,4}\left(t w_{x,3}(w_{x,3}^2 + w_{y,3}^2) w_{3,4}^2 + x w_{x,3} + y w_{y,3}\right)\right) \\ &+ w_{5,u} \operatorname{sech}\left(y\left(w_{1,5} w_{y,1} + w_{2,5} w_{y,2} + w_{3,5} w_{y,3}\right)\right) \end{aligned} \tag{18}$$

In order to fully demonstrate the dynamic characteristics of the solution of Equation (18), we provided its three-dimensional graphs, contour diagram, thermal map, and evolution plot (**Figure 7**). The solution Equation (18) describes a stable periodic oscillation mode. The sine function in its mathematical structure governs the regular periodic changes, while the hyperbolic secant function makes the oscillation spatially localized. As can be seen from the evolution diagram, the waveform maintains its amplitude and shape during propagation, demonstrating good energy locality and time periodicity. It can be considered a type of stable coherent structure that can be maintained for a long time in nonlinear systems.

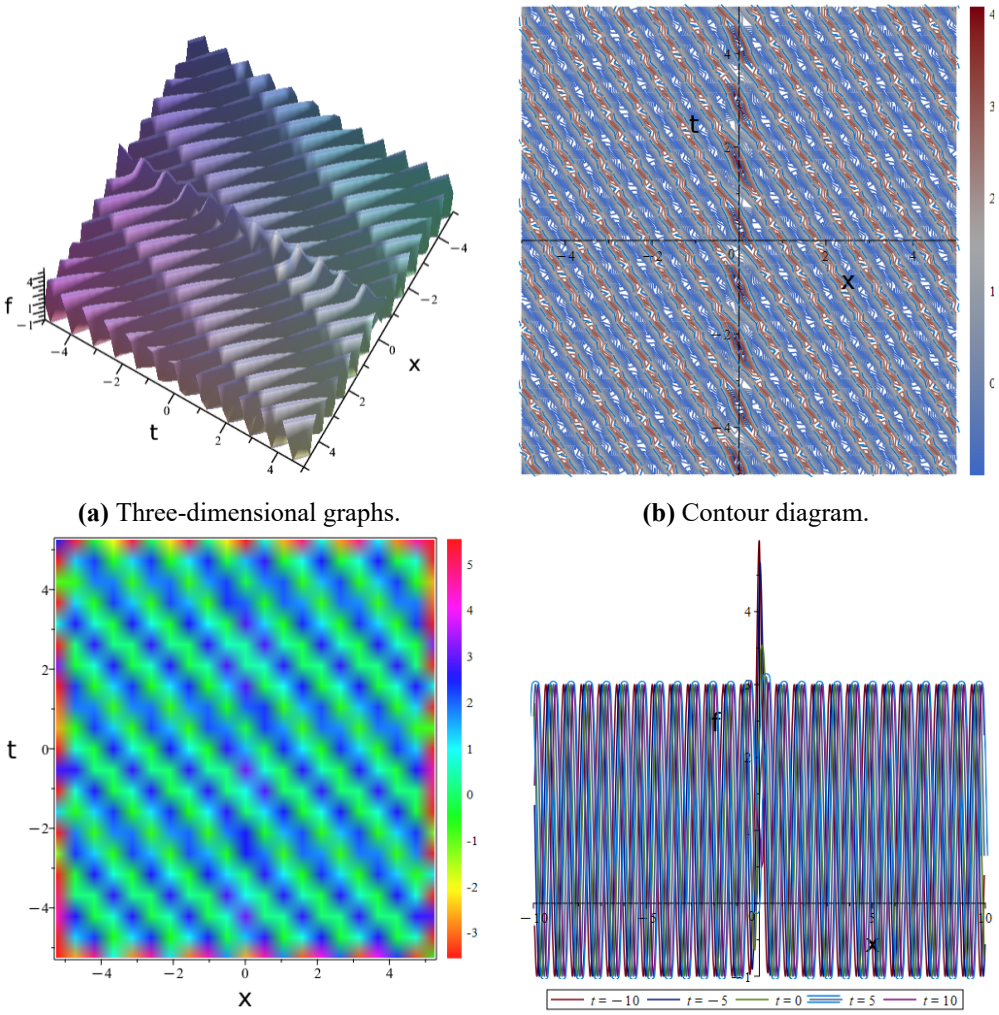

(a) Three-dimensional graphs. **(b)** Contour diagram.

(c) Thermal map. **(d)** Evolution plot.

Figure 7. Three-dimensional graphs, contour diagram, thermal map, and evolution plot of Equation (18) at $b_6 = 1, w_{4,u} = 2, w_{3,4} = 2, w_{x,3} = 2, w_{y,1} = 2, w_{y,2} = 2, w_{y,3} = 2, w_{1,5} = 2, w_{3,5} = 2, w_{5,u} = 2, w_{2,5} = 2$.

4.3. Model[3-3-2-1]-3

The network model structure is similar to the above section, the difference is that the activation function of the second hidden layer has changed. Letting $F_4(\xi_4) = \text{sech}(\xi_4)$, $F_5(\xi_5) = \tanh(\xi_5)$. By the deep neural network Model[3-3-2-1]-3,we can obtain:

$$\begin{aligned} f \quad &= b_6 + w_{4,u} \cdot \text{sech}(w_{t,4}(t \cdot w_{t,1} + x w_{x,1} + y w_{y,1}) \\ &+ w_{2,4} \cdot (t \cdot w_{t,2} + x \cdot w_{x,2} + y w_{y,2}) \\ &+ w_{3,4} \cdot (t \cdot w_{t,3} + x \cdot w_{x,3} + y w_{y,3}) \\ &+ w_{5,u} \cdot \tanh(w_{1,5} \cdot (t \cdot w_{t,1} + x w_{x,1} + y w_{y,1}) \\ &+ w_{2,5} \cdot (t \cdot w_{t,2} + x \cdot w_{x,2} + y w_{y,2}) \\ &+ w_{3,5} \cdot (t \cdot w_{t,3} + x \cdot w_{x,3} + y w_{y,3}) \end{aligned} \tag{19}$$

Substitute Equation (19) into nonlinear PDE (1), 5 solutions can be obtained, one

of the solutions is as follows,

$$\begin{aligned}
&\{w_{1,4}=0, w_{1,5}=w_{1,5}, w_{2,4}=w_{2,4}, w_{2,5}=w_{2,5}\\
&w_{3,4}=w_{3,4}, w_{3,5}=w_{3,5}, w_{4,4}=w_{4,4}, w_{5,4}=w_{5,4}\\
&w_{t,1}=-\frac{w_{t,3}(w_{2,4}w_{3,5}-w_{2,5}w_{3,4})}{w_{2,4}w_{1,5}}\\
&w_{t,2}=-\frac{w_{3,4}w_{t,3}}{w_{2,4}}, w_{t,3}=w_{t,3}\\
&w_{x,1}=-\frac{w_{x,3}(w_{2,4}w_{3,5}-w_{2,5}w_{3,4})}{w_{1,5}w_{2,4}}\\
&w_{x,2}=-\frac{w_{3,4}w_{x,3}}{w_{2,4}}, w_{x,3}=w_{x,3}\\
&w_{y,1}=w_{y,1}, w_{y,2}=w_{y,2}, w_{y,3}=w_{y,3}\}
\end{aligned} \tag{20}$$

By substituting Equation (20) into Equation (19), the solution of the original equation can ultimately be obtained as:

$$\begin{aligned}
f: \quad &= b_6 + w_{4,u}\tanh\left(y\left(w_{2,4}w_{y,2}+w_{3,4}w_{y,3}\right)\right)\\
&+w_{5,u}\,\mathrm{sech}\left(y\left(w_{1,5}w_{y,1}+w_{2,5}w_{y,2}+w_{3,5}w_{y,3}\right)\right)
\end{aligned} \tag{21}$$

The solution Equation (21) describes a static field with a stable nonlinear structure in space. Its mathematical form consists of the superposition of hyperbolic tangent and hyperbolic secant functions, corresponding to the smooth transition layer and localized peak in the waveform, respectively. The subplots in **Figure 8** consistently show that the field maintains a strictly static distribution in the spatiotemporal dimension, and the complete overlap of the curves at different times in the evolution diagram verifies its time independence. This solution characterizes a stable equilibrium state of the system under specific parameters and can be used as a static solution to describe the spatial modulation background field in certain physical systems.

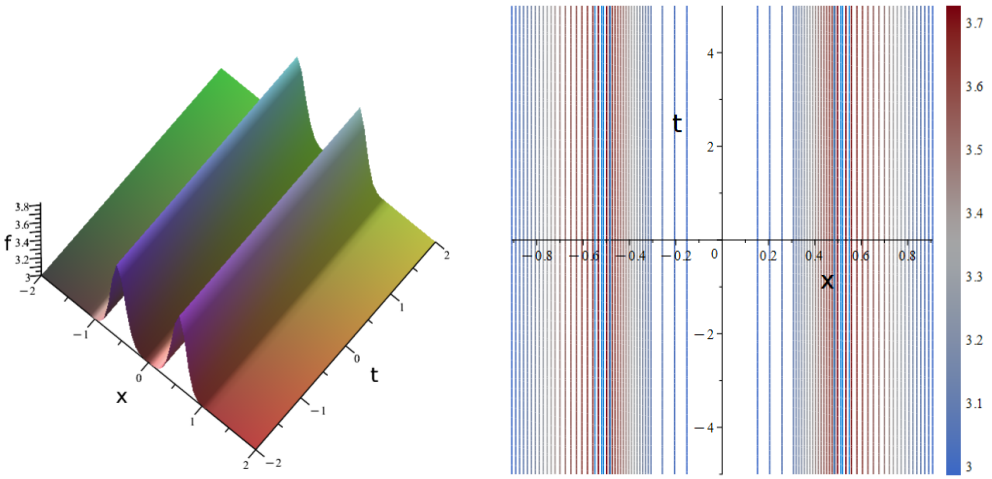

(a) Three-dimensional graphs. **(b)** Contour diagram.

Figure 8. *Cont.*

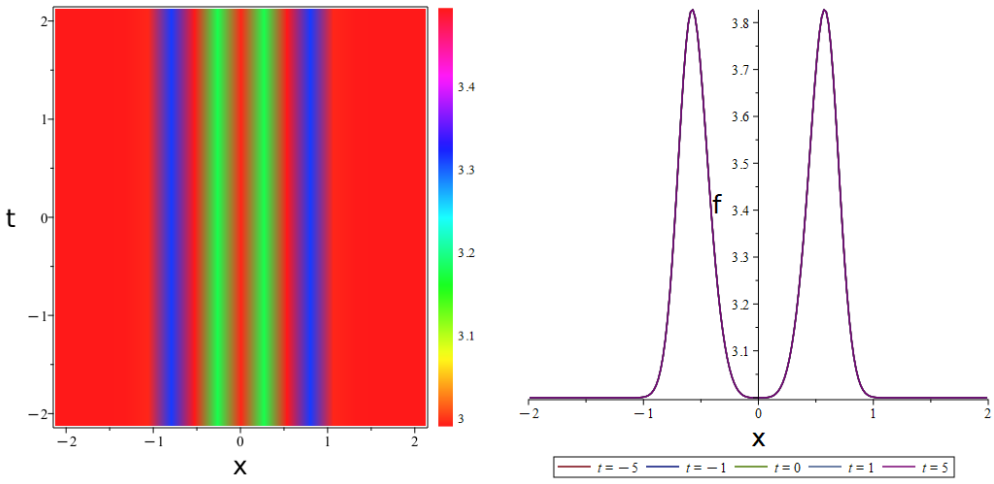

(c) Thermal map. **(d)** Evolution plot.

Figure 8. Three-dimensional graphs, contour diagram, thermal map, and evolution plot of Equation (21) at $b_6 = 1, w_{4,u} = 2, w_{3,4} = 2, w_{x,3} = 2, w_{y,1} = 2, w_{y,2} = 2, w_{y,3} = 2, w_{1,5} = 2, w_{3,5} = 2, w_{5,u} = 2, w_{2,5} = 2$.

5. Conclusion

This study establishes a neural network-symbolic computing framework for deriving analytical solutions to nonlinear partial differential equations. By leveraging the adaptive architecture of neural networks together with the precision of symbolic computation, the approach mitigates the limitations inherent in purely numerical or symbolic methods while improving generality. Its effectiveness is demonstrated through the solution of the (2+1)-dimensional Boiti–Leon–Manna–Pempinelli (BLMP) equation, from which multiple previously unreported analytical solutions are obtained and their dynamic features visualized. In contrast to conventional numerical techniques such as finite-difference or pseudo-spectral methods, the present framework yields closed-form analytical expressions, effectively avoiding discretization errors. Furthermore, it operates without dependence on specialized mathematical techniques such as bilinear transforms or Darboux transformations, which are often equation-specific and algebraically complex. Compared with physics-informed neural networks, the proposed method does not incorporate physical constraints into the loss function, reduces computational resource requirements, and preserves interpretability through symbolic representation. The BLMP equation, which models notable phenomena in fluid dynamics and nonlinear wave propagation, has yet to be treated using such a neural-symbolic strategy. Our results indicate that this hybrid methodology can effectively reveal exact solutions and dynamical properties that are difficult to access through traditional means. Future efforts will focus on extending the framework to more intricate nonlinear systems and exploring integration with graph neural networks for problems involving irregular domains. This work thus offers an efficient, interpretable, and scalable alternative for solving nonlinear PDEs, with potential applications in areas such as nonlinear optics, plasma physics, and engineering dynamics.

Author contributions: Conceptualization, JLS and RFZ; methodology, JLS; software, JLS and JEH; validation, JLS, JBL and RFZ; formal analysis, JLS; investigation, JLS; resources, RFZ and YG; writing—original draft preparation, JWH and JBL; writing—review and editing, JLS; visualization, JLS and JWH; supervision, RFZ; project administration, YG; funding acquisition, JLS. All authors have read and agreed to the published version of the manuscript.

Funding: This work was supported by the Open Research Fund of Computational Physics Key Laboratory of Sichuan Province, Yibin University (No.YBUJSWL-KX-2025-04), Tianyuan Fund for Mathematics of the National Natural Science Foundation of China (Grant No.12426105), Fundamental Research Program of Shanxi Province (No. 202403021222001), the Scientific and Technological Innovation Programs (STIP) of Higher Education Institutions in Shanxi (No.2024L022), Funded by Open Foundation of Hubei Key Laboratory of Applied Mathematics (Hubei University) under the No.HBAM202401, the Wen Ying Young Scholars Talent Project of Shanxi University (No. 138541088), the Training Program of Yibin University (No.2024XJPY13) and Sailing Project of Yibin University (No.2024XJQH04).

Institutional review board statement: Not applicable.

Informed consent statement: Not applicable.

Data availability statement: Data availability is not applicable to this article as no new data were created or analyzed in this study.

Conflict of interest: The authors declare no conflict of interest.

References

1. Cevikel AC. New solutions for the high-dimensional fractional BLMP equations. Journal of Ocean Engineering and Science. 2022; 7: 592–600. doi: 10.1016/j.joes.2022.06.023
2. Kumar S, Kumar A. Abundant closed-form wave solutions and dynamical structures of soliton solutions to the (3+1)-dimensional BLMP equation in mathematical physics. Journal of Ocean Engineering and Science. 2022; 7(2): 178–187. doi: 10.1016/j.joes.2021.08.001
3. Lan ZZ. Multi-soliton solutions for a (2+1)-dimensional variable-coefficient nonlinear Schrödinger equation. Applied Mathematics Letters. 2018; 86: 243–248. doi: 10.1016/j.aml.2018.05.014
4. Lan ZZ, Guo BL. Nonlinear waves behaviors for a coupled generalized nonlinear Schrödinger–Boussinesq system in a homogeneous magnetized plasma. Nonlinear Dynamics. 2020; 100: 3771–3784. doi: 10.1007/s11071-020-05716-1
5. Ma WX. Lump waves in a spatial symmetric nonlinear dispersive wave model in (2+1)-dimension. Mathematics. 2023; 11(22): 4664. doi: 10.3390/math11224664
6. Ma WX. A combined derivative nonlinear Schrödinger soliton hierarchy. Reports on Mathematical Physics. 2024; 93(3): 313–325. doi: 10.1016/S0034-4877(24)00040-5
7. Wang X, Yang Y, Kou W, et al. Analytical solution of Balitsky-Kovchegov equation with homogeneous balance method. Physical Review D. 2021; 103: 056008. doi: 10.1103/physrevd.103.056008
8. Constantin A, Gerdjikov VS, Ivanov RI. Inverse scattering transform for the Camassa–Holm equation. Inverse Problems. 2006; 22(6): 2197–2207. doi: 10.1088/0266-5611/22/6/017
9. Yin YH, Lü X, Ma WX. Bäcklund transformation, exact solutions and diverse interaction phenomena to a (3+1)-dimensional nonlinear evolution equation. Nonlinear Dynamics. 2022; 108: 4181–4194. doi: 10.1007/s11071-021-06531-y
10. Baber MZ, Bittaye E, Ahmad H, et al. Dynamical behavior of synchronized symmetric waves in the two-mode Chaffee-Infante model via Hirota bilinear transformation. Results in Engineering. 2025; 27: 106328. doi:

10.1016/j.rineng.2025.106328
11. Li Y, Yao R, Lou S. An extended Hirota bilinear method and new wave structures of (2+1)-dimensional Sawada–Kotera equation. Applied Mathematics Letters. 2023; 145: 108760. doi: 10.1016/j.aml.2023.108760
12. Barik S, Behera S. Soliton dynamics of the phi-four equation and Fisher equation by Hirota bilinear method. International Journal of Applied and Computational Mathematics. 2025; 11(6): 243. doi: 10.1007/s40819-025-02055-w
13. Kumar M, Tiwari AK. Soliton solutions of BLMP equation by Lie symmetry approach. Computers and Mathematics with Applications. 2018; 75(4): 1434–1442. doi: 10.1016/j.camwa.2017.11.018
14. Kumar R, Tanwar DV, Singh SG, et al. Lie symmetry reductions and exact solutions of (2+1)-dimensional Boiti–Leon–Manna–Pempinelli equation in shallow water. Canadian Journal of Physics. 2025; 103(6): 245–254. doi: 10.1139/cjp-2024-0257
15. Wu XH, Gao YT, Yu X, et al. Modified generalized Darboux transformation and solitons for a Lakshmanan–Porsezian–Daniel equation. Chaos, Solitons and Fractals. 2022; 162: 112399. doi: 10.1016/j.chaos.2022.112399
16. Yue C, Khater MMA, Inc M, et al. Abundant analytical solutions of the fractional nonlinear (2+1)-dimensional BLMP equation arising in incompressible fluid. International Journal of Modern Physics B. 2020; 34(9): 2050084. doi: 10.1142/S0217979220500848
17. Darvishi MT, Najafi M, Arbabi SB, et al. New extensions of (2+1)-dimensional BLMP models with soliton solutions. Optical and Quantum Electronics. 2023; 55: 568. doi: 10.1007/s11082-023-04862-1
18. Gilson CR, Nimmo JJC, Willox RA. A (2+1)-dimensional generalization of the AKNS shallow water wave equation. Physics Letters A. 1993; 180(4–5): 337–345. doi: 10.1016/0375-9601(93)91187-A
19. Tang YN, Zai WJ. New periodic-wave solutions for (2+1)- and (3+1)-dimensional Boiti–Leon–Manna–Pempinelli equations. Nonlinear Dynamics. 2015; 81: 249–255. doi: 10.1007/s11071-015-1986-4
20. Qi JX, An HL, Jin P. Breather molecules and localized interaction solutions in the (2+1)-dimensional BLMP equation. Communications in Theoretical Physics. 2021; 73: 125005. doi: 10.1088/1572-9494/ac2f2b
21. He JL, Han YT, Xu T, et al. Solitons, lump and interactional solutions of the (3+1)-dimensional BLMP equation in incompressible fluid. Physica Scripta. 2022; 99(8): 085267. doi: 10.1088/1402-4896/ad651a
22. Jisha CR, Dubey RK. Wave interactions and structures of (4+1)-dimensional Boiti–Leon–Manna–Pempinelli equation. Nonlinear Dynamics. 2022; 110: 3685–3697. doi: 10.1007/s11071-022-07816-6
23. Huang C, Zhu Y, Li K, et al. M-lump solutions, lump-breather solutions, and N-soliton wave solutions for the KP-BBM equation via the improved bilinear neural network method using innovative composite functions. Nonlinear Dynamics. 2024; 112: 21355–21368. doi: 10.1007/s11071-024-10122-y
24. Chou D, Rehman HU, Awan AU, et al. Investigating soliton phenomena in incompressible fluids: Study of the (2+1)-dimensional Boiti–Leon–Manna–Pempinelli equation. Modern Physics Letters A. 2025; 40(15): 2550049. doi: 10.1142/s021773232550049x
25. Qin CY, Zhang RF, Li YH. Various exact solutions of the (4+1)-dimensional Boiti–Leon–Manna–Pempinelli-like equation by using bilinear neural network method. Chaos, Solitons and Fractals. 2024; 187: 115438. doi: 10.1016/j.chaos.2024.115438
26. Shen JL, Wu XY. Periodic-soliton and periodic-type solutions of the (3+1)-dimensional Boiti–Leon–Manna–Pempinelli equation by using bilinear neural network method. Nonlinear Dynamics. 2021; 106: 831–840. doi: 10.1007/s11071-021-06848-8
27. Zhang RF, Li MC, Cherraf A, et al. The interference wave and the bright and dark soliton for two integro-differential equation by using bilinear neural network method. Nonlinear Dynamics. 2023; 111: 8637–8646. doi: 10.1007/s11071-023-08257-5
28. Bilige S, Shao H, Wang X. Abundant solutions and superposition behavior analysis of a (3+1)-dimensional Boiti–Leon–Manna–Pempinelli equation. Mathematical Methods in the Applied Sciences. 2025; 48(14): 13368–13379. doi: 10.1002/mma.11108
29. Raissi M, Perdikaris P, Karniadakis GE. Physics-informed neural networks: A deep learning framework for solving forward and inverse problems involving nonlinear partial differential equations. Journal of Computational Physics. 2019; 378: 686–707. doi: 10.1016/j.jcp.2018.10.045
30. Wang S, Teng Q, Perdikaris P. Understanding and mitigating gradient pathologies in physics-informed neural networks. SIAM Journal on Scientific Computing. 2021; 43(5): A3055–A3081. doi: 10.1137/20m1318043
31. Mishra S, Molinaro R. Estimates on the generalization error of physics-informed neural networks for approximating

a class of inverse problems for PDEs. IMA Journal of Numerical Analysis. 2022; 42(2): 981–1022. doi: 10.1093/imanum/drab032

32. Geneva N, Zabaras N. Modeling the dynamics of PDE systems with physics-constrained deep auto-regressive networks. Journal of Computational Physics. 2020; 403: 109056. doi: 10.1016/j.jcp.2019.109056
33. Pang G, Lu L, Karniadakis GE. fPINNs: Fractional physics-informed neural networks. SIAM Journal on Scientific Computing. 2019; 41(4): A2603–A2626. doi: 10.1137/18m1229845
34. Xie XR, Zhang RF. Neural network-based symbolic calculation approach for solving the Korteweg–de Vries equation. Chaos, Solitons and Fractals. 2025; 194: 116232. doi: 10.1016/j.chaos.2025.116232